Available online at www.sciencedirect.com
ScienceDirect
Advances in Space Research 46 (2010) 1064–1069
ADVANCES IN SPACE RESEARCH (a COSPAR publication)
www.elsevier.com/locate/asr

Longitudinal behaviors of the IRI-B parameters of the equatorial electron density profiles retrieved from FORMOSAT-3/COSMIC radio occultation measurements

Libo Liu *, Weixing Wan, Baiqi Ning, Man-Lian Zhang, Maosheng He, Xinan Yue

Beijing National Observatory of Space Environment, Institute of Geology and Geophysics, Chinese Academy of Sciences, Beijing 100029, PR China

Received 27 August 2009; received in revised form 17 September 2009; accepted 17 September 2009

Abstract

The electron density profiles in the bottomside F_2-layer ionosphere are described by the thickness parameter $B0$ and the shape parameter $B1$ in the International Reference Ionosphere (IRI) model. We collected the ionospheric electron density (N_e) profiles from the FORMOSAT-3/COSMIC (F3/C) radio occultation measurements from DoY (day number of year) 194, 2006 to DoY 293, 2008 to investigate the daytime behaviors of IRI-B parameters ($B0$ and $B1$) in the equatorial regions. Our fittings confirm that the IRI bottomside profile function can well describe the averaged profiles in the bottomside ionosphere. Analysis of the equatorial electron density profile datasets provides unprecedented detail of the behaviors of $B0$ and $B1$ parameters in equatorial regions at low solar activity. The longitudinal averaged $B1$ has values comparable with IRI-2007 while it shows little seasonal variation. In contrast, the observed $B0$ presents semi-annual variation with maxima in solstice months and minima in equinox months, which is not reproduced by IRI-2007. Moreover, there are complicated longitudinal variations of $B0$ with patterns varying with seasons. Peaks are distinct in the wave-like longitudinal structure of $B0$ in equinox months. An outstanding feature is that a stable peak appears around 100°E in four seasons. The significant longitudinal variation of $B0$ provides challenges for further improving the presentations of the bottomside ionosphere in IRI.

Keywords: Ionosphere; Equatorial ionosphere; Modeling and forecasting; Plasma temperature and density

1. Introduction

The most famous and widely used empirical model of the ionosphere is the International Reference Ionosphere (IRI), which specifies the monthly average distributions of the ionosphere. The IRI model has been developed and updated by a joint working group of Committee on Space Research (COSPAR) and the International Union of Radio Science (URSI) for decades (e.g., Bilitza, 1990). The IRI adopts the analytical function

$$N_e(h) = \frac{N_m F2 \exp(-x^{B_1})}{\cosh(x)}, \quad x = \frac{h_m F2 - h}{B_0} \tag{1}$$

to describe the ionospheric electron density profile $N_e(h)$ below the peak height ($h_m F2$) of the F_2-layer (see Bilitza, 1990). $N_m F2$ in Eq. (1) is the peak electron density of the F_2-layer; $B0$ is the thickness parameter measuring the bottomside F_2-layer profile thickness; and $B1$ is the shape parameter determining the shape of the profile between $h_m F2$ and $h_{0.238}$ (the height where the values of N_e drops to $0.238 N_m F2$). The IRI-B parameters ($B0$ and $B1$) are two key parameters used in IRI to specify the ionospheric electron density profiles in the bottomside F_2-layer. There are two options available in the IRI model; that is, the standard table option (Bilitza, 1990; Bilitza et al., 2000) and Gulyaeva's option (see Gulyaeva, 1987).

Since the bottomside F_2-layer profiles critically depend on the IRI-B parameters in addition to $N_m F2$ and $h_m F2$, there are many studies conducted to explore the behaviors

* Corresponding author.
E-mail address: liul@mail.iggcas.ac.cn (L. Liu).

0273-1177/$36.00 © 2010 COSPAR. Published by Elsevier Ltd. All rights reserved.
doi:10.1016/j.asr.2010.06.005

of the IRI-B parameters at different locations in the past years (e.g., Adeniyi and Radicella, 1998; Altadill et al., 2008; Batista and Abdu, 2004; Blanch et al., 2007; Chen et al., 2006; McKinnell et al., 2009; Mosert, 1998; Obrou et al., 2005; Sethi et al., 2009; Zhang et al., 2000, 2008; Zhang and Huang, 1998). Attempts are also made to validate and improve the predictability of IRI parameters after its first release in 1978 (e.g., Bilitza et al., 2000; Gulyaeva, 1987; Lee et al., 2008; Mahajan and Sethi, 2001; Radicella et al., 1998; Reinisch and Huang, 1998; Sethi et al., 2003; Zhang et al., 2000, 2007; Zhang and Huang, 1998). Altadill et al. (2009) made a try to overcome the scarcity of data via extracting the bottomside parameters covering the time interval from 1998 to 2006 at world-wide 27 ionosonde stations, but their results may possibly hide some longitudinal effects. These works were conducted mainly with ground-based observations, such as ionosondes and incoherent scatter radars. It is reported that there are some limitations in the IRI model, due to uneven data coverage as well as the complicated behaviors of the ionosphere. For example, there are scare ground observations over oceanic regions and in global equatorial regions.

Some of previous researches have showed some shortcomings of both options of the IRI-B parameters (e.g., Lee et al., 2008; Zhang et al., 2008), particularly in the equatorial and low latitudes. Under the framework of the ICTP Task Force Activities, new table values of $B0$ and $B1$ have been developed to update the old one in the IRI (Bilitza et al., 2000; Radicella et al., 1998). Besides searching for better $B0$ and $B1$ (Reinisch and Huang, 1998), more observations with different techniques and at global locations are certainly required to be digested for improving the IRI model, especial for the equatorial region. As we know, the equatorial region is one of the most important parts of the ionosphere because it contains the highest amount of electrons in the ionosphere. Moreover, the daytime plasma fountain effect produces the equatorial ionization anomaly, which provides unique challenges for empirical modeling the equatorial ionosphere. The predictions of the IRI-B parameters have been examined with some equatorial observations at Jicamarca (76.9°W, dip latitude 1°N), Korhogo (5.4°W, dip −0.67°), Ouagadougou (1.5°W, dip latitude 5.9°N), and São Luís (44.2°W, dip latitude 4.5°S) (Adeniyi and Radicella, 1998; Batista and Abdu, 2004; Lee et al., 2008; Obrou et al., 2005). Large discrepancies are still found between the observations and the IRI model. Further, recent investigations indicate a strong longitudinal variation of N_e (e.g., Lin et al., 2007; Wan et al., 2008), electron temperature (Ren et al., 2008), and plasma gradient scale height (Liu et al., 2008) in equatorial ionosphere. It is truly a question whether the IRI-B parameters in such a narrow longitudinal range can represent for their behaviors in global equatorial regions. In other words, does $B0$ show strong longitudinal variations as in electron density, drift velocity, plasma temperature and scale height? Therefore, more equatorial ionospheric data at different longitudes are required to reveal the characteristics of these parameters and also to validate and enhance the predictability of the IRI.

In this report, we collect the N_e profiles from the FORMOSAT-3/COSMIC (a Constellation Observing System for Meteorology, Ionosphere, and Climate mission; F3/C, for short) ionospheric radio occultation (IRO) observations during the interval from DoY (day number of year) 194, 2006 to DoY 293, 2008 which are archived at University Corporation for Atmospheric Research (UCAR, USA) to investigate the behaviors of the IRI-B parameters over global equatorial regions. F3/C registered up to 2600 occultation events per day. With this huge database of F3/C IRO N_e profiles, we conduct a statistical analysis on the equatorial behaviors of IRI-B parameters. Our emphasis is on their seasonal and longitudinal features during the daytime. The most significant feature in our results is the wave-like longitudinal pattern in daytime equatorial $B0$, which is not detected before yet.

2. Data source and processing

The F3/C was launched on 15 April 2006 in a circular low-Earth orbit originally at 512 km altitude with a 72° inclination. The F3/C consists of six microsatellites which are currently operating at around 800 km altitude and 30° separation in longitude between each satellite. Electron density profiles of the ionosphere can be retrieved from the F3/C IRO measurements (e.g., Lei et al., 2007; Lin et al., 2007). The reader is referred to Lei et al. (2007) for a detail description on the F3/C mission and IRO N_e profile inversion technique. The F3/C has already had a significant impact on various fields of ionospheric physics and meteorology.

Similar to that of Liu et al. (2008, 2009), the F3/C N_e data collected for this investigation are obtained from the COSMIC Data Analysis and Archive Center (CDAAC) of UCAR. We collect the F3/C N_e data during the interval from DoY 194, 2006 to DoY 293, 2008 to investigate the behaviors of the IRI-B parameters ($B0$ and $B1$) in equatorial regions. The data distribution of the F3/C N_e dataset has been introduced by Liu et al. (2008). During this interval the solar 10.7 cm flux $F_{10.7}$ was quite low. Therefore, we will ignore the possible solar cycle effects when we examine the average behaviors of the ionosphere during this period.

We fit individual density profiles with Chapman-α function in a least-squares sense. A related coefficient and the ratio of mean square root between the fitted profile and data to 20 and 80 percentiles of each profile can be obtained from the above fitting processing. According to the related coefficient and the relative mean square roots, we discard some bad profiles, about 5% of all profiles. After rejected those N_e profiles with poor data quality, we apply a 7-point moving smooth to individual N_e profiles and interpolate the data to regular altitude levels (170–500 km with a step of 2 km). To obtain the general daytime patterns, we select data points with dip angles in the range of ±7° for the following analysis. The daytime equatorial N_e points are sorted in month bins. When we explore the

longitudinal behavior, we further split data points into sub-bins according to their geographic longitudes.

It is reported that electron density profiles N_e(h) in the F_2-region can be reasonably represented in terms of the Chapman function (see Liu et al., 2007, and references cited therein)

$$N_e(h) = N_m\mathrm{F2}\exp\left\{\frac{1}{2}\left[1-\frac{h-h_m\mathrm{F2}}{H_m}-\exp\left(-\frac{h-h_m\mathrm{F2}}{H_m}\right)\right]\right\}. \quad (2)$$

If we assume that the F_2-region N_e profiles can be approximated by Eq. (2), the peak parameters (h_mF2, N_mF2, and the Chapman scale height H_m) for each bin can be extracted from the data points in a least-squares sense. When the peak parameters (h_mF2 and N_mF2) have been determined, the IRI-B parameters ($B0$ and $B1$) for each bin are then deduced from the bottomside data points via applying a least-square fitting in terms of Eq. (1). To provide ample points for a reliable fitting, (1) the size of the bins is chosen to be one month around 13:00 LT, when we consider the general behavior of the IRI-B parameters (i.e., ignore the possible longitudinal dependence); (2) two months data in the time interval of 12:00–14:00 LT are binned together, if the longitudinal effect is explored.

As an example, Fig. 1 shows the altitude variation of equatorial electron densities around 13:00 LT in April. The blue dots in Fig. 1 are the electron density data from the F3/C global observations with dip angles in the range of ±7° around 13:00 LT in April. We set the lower altitude limit of the data to 170 km. The grey curve shows the result fitted with a Chapman-α profile function (Eq. (2)) in a least-squares sense, while the red curve represents the fitting with the IRI bottomside profile function (Eq. (1)).

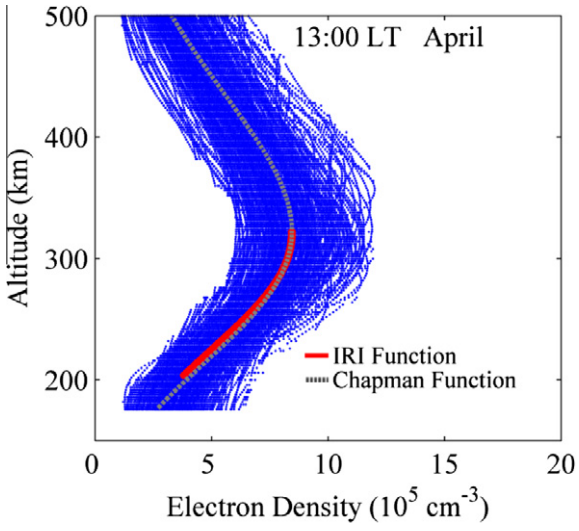

Fig. 1. The equatorial electron density data of the F3/C global observations within 1 h around 13:00 LT in April. The grey curve shows the fitting results with a Chapman-α profile function, while the red curve represents the fitting with the IRI bottomside profile function (see Eq. (1) in the text). (For interpretation of the references to color in this figure legend, the reader is referred to the web version of this paper.)

For the latter analysis, the fitting covered an altitude range between h_mF2 and h_mF2-120 km. It can be seen that, Chapman-α profile function can well represents the average F3/C electron density profile in the altitudinal range of 170–500 km, and Eq. (1) can reasonably describe the average bottomside F_2-layer profile. It supports that the conclusion of Reinisch and Huang (1998); they speculated that wrong values of $B0$ and $B1$ are responsible for the large deviations of IRI values from observations, rather than limitations of Eq. (1) in functional description of the bottomside profiles. Moreover, an important feature is a moderate spread in electron densities around the average profile at all altitudes, partly due to the day-to-day variability and complicated longitudinal dependency of the ionosphere. We just explore the daytime behavior, take 13:00 LT for instance in this report.

3. Seasonal variation of the parameters ($B0$ and $B1$)

Fig. 2 shows the seasonal variation of the monthly $B0$ and $B1$ parameters around 13:00 LT in dip equatorial region. The $B1$ and $B0$ parameters are averaged over all geographical longitudes. The top and middle panels of Fig. 2 illustrate the $B1$ and $B0$ deduced from the equatorial F3/C IRO electron density observations at all longitudes, and the bottom panel depicts the $B0$ values predicted by the IRI-2007 model (Bilitza and Reinisch, 2008). The $B0$ provided by the IRI standard table option is represented with solid line, and that of Gulyaeva's option in dashed curve with dots.

At midday, the observed $B1$ has highest values in March equinox months and lowest values in solstice months. The longitudinal averaged values of the parameter $B1$ at 13:00 LT varies from 1.8 in January to 2.3 in March. In contrast, Adeniyi and Radicella (1998) found daytime $B1$ at Ouagadougou (1.5°W, dip 5.9°N) at low solar activity having a fairly constant value of 1.7. Bilitza et al. (2000) calculated the average $B1$ at Ouagadougou and, Korhogo. They found that $B1$ exhibits little change with season and solar activity. As a result, the $B1$ in the new IRI takes a value of 1.9 during the daytime. Further, no seasonal effect is included for equatorial $B1$ in IRI.

The observed equatorial $B0$ takes values varying from 154.5 km to 182.6 km. The middle panel of Fig. 2 shows that, there is an obvious semiannual variation in the observed $B0$ during the daytime, with higher values in solstice months and lower values in March and September equinox months. It indicates that the average profiles for the bottomside F_2-layer have a seasonal trend, being thinner in equinox months and thicker in solstice months. This seasonal feature of the observed $B0$ is opposite to that of the F_2-layer peak density N_mF2 (Liu et al., 2009). Daytime N_mF2 presents a significant semiannual variation with maxima in equinox months and minima in solstice months.

Lee et al. (2008) also provided a seasonal pattern of equatorial $B0$ at low solar activity by analyzing the ionograms at Jicamarca in 1996. Their work demonstrated $B0$

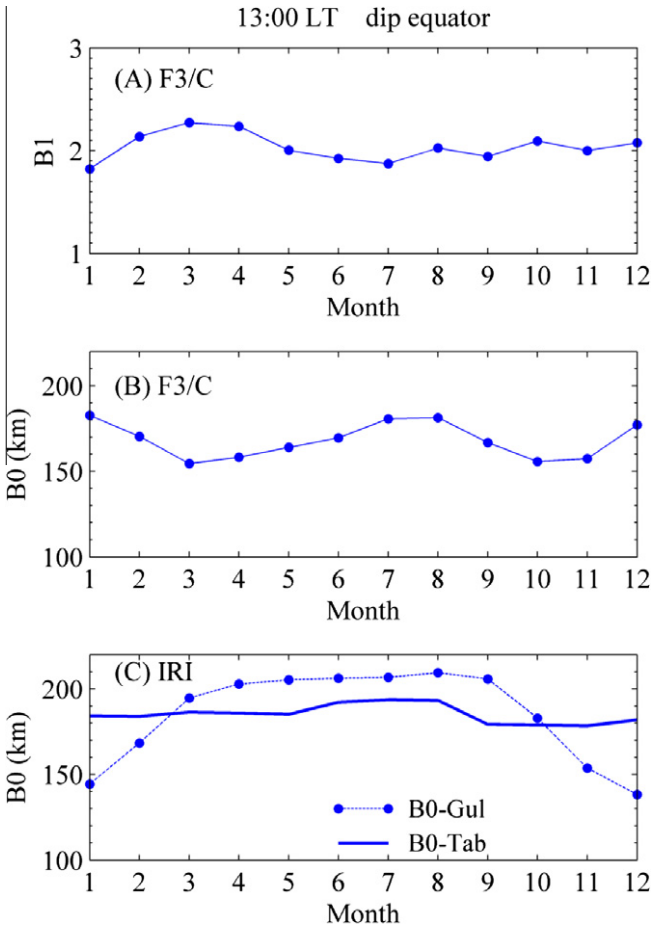

Fig. 2. Seasonal variation of (A) $B1$ and (B) $B0$ deduced from the global F3/C IRO electron density profiles around the dip equator at 13:00 LT during the interval from DoY (day of year) 194, 2006 to DoY 293, 2008. (C) Seasonal variation of IRI $B0$ at dip equator at 13:00 LT. The dashed curve with dots shows the values of Gulyaeva's option of $B0$, while the solid line illustrates that of the IRI standard table option.

at Jicamarca mainly of an annual component with a July–August maximum. However, a secondary peak can also be seen in December and January. Moreover, the seasonal pattern of daytime $B0$ presented in Lee et al. (2008) can be reproduced with the F3/C data, if we analyze those data with longitudes around that of Jicamarca. The difference of our result from Lee et al. (2008) may partly or mainly come from the longitudinal structure of $B0$. A question naturally arises: what is the longitudinal dependency of $B0$? It will be addressed in the next section.

Discrepancy in the seasonal variation of equatorial $B0$ is found between our observational result and IRI. As the third panel of Fig. 2 illustrated, the IRI table option (the solid line) has a roughly comparable value with the observations, but the latter has larger semiannual trend. In contrast, the Gulyaeva's option (dashed curve with dots) provides a seasonal variation mainly with an annual component. In equatorial region, Gulyaeva's $B0$ has lowest values (138 km) in December solstice months and highest values (209 km) in June solstice months. It should be mentioned that, in IRI, the seasonal variation of $B0$ is opposite in both geographic hemispheres; that is, $B0$ in the southern hemisphere is assumed to simply have a phase shift of 6 months, compared to the northern hemisphere.

4. Longitudinal behavior of the $B0$ parameter

As mentioned before, the longitudinal pattern of $B0$ is not known yet due to insufficient data coverage. We explore the longitudinal behavior of $B0$ by evaluating the median values of $B0$ with the equatorial N_e data points within 2 h around 13:00 LT in the given geographic longitude and DoY bins. Fig. 3 depicts the longitudinal variation of daytime equatorial $B0$ for four seasons. From Fig. 3, we can see a complicated longitudinal structure in equatorial $B0$, which is strongly variable with season. In other words, the seasonal differences of $B0$ are dependent on longitude. Naturally the seasonal variation of $B0$ at Jicamarca (Lee et al., 2008) is slightly different from that of our longitudinal averaged result. In contrast, no regular longitudinal structure can be detected in $B1$, as illustrated

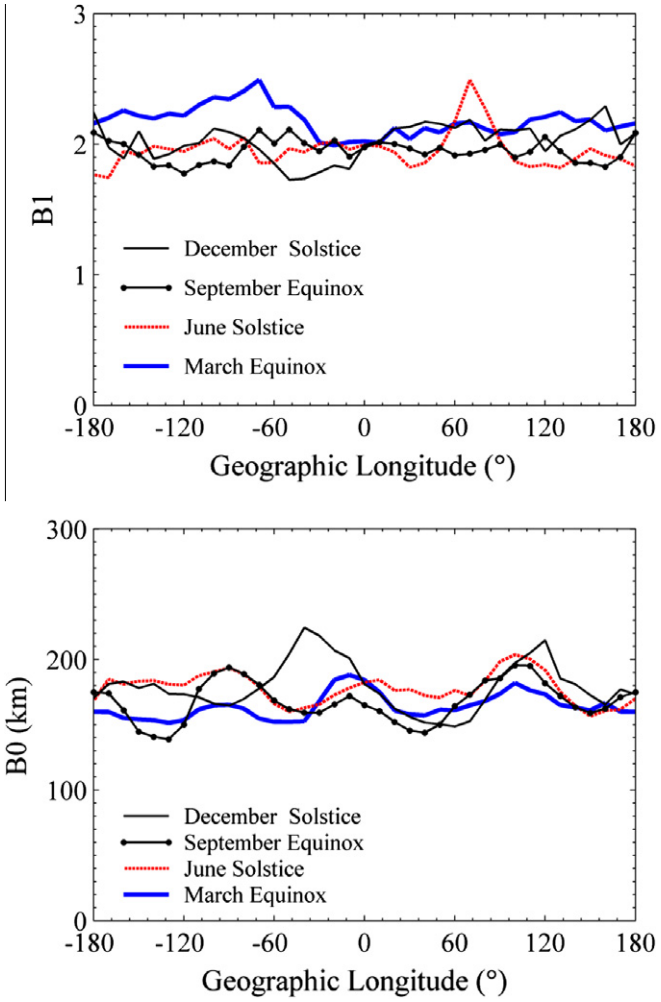

Fig. 3. Longitudinal variation of daytime $B0$ and $B1$ around the dip equator in four seasons. The $B0$ and $B1$ are deduced from the F3/C IRO electron density profiles around the dip equator during the interval from DoY (day of year) 194, 2006 to DoY 293, 2008.

in the upper panel of Fig. 3. Therefore, it requires more data from different longitudes for IRI to improve its presentation of the bottomside ionospheric profiles.

Overall, during daytime the longitudinal structure of the observed equatorial $B0$ presents a wave-like pattern, which has amplitude comparable to that of the seasonal variation. The presence of a wavenumber-four structure in $B0$ is clearly detected in March and September equinoxes. In contrast, there are three distinct peaks in the longitudinal variations of $B0$ in June and December solstices. An interesting feature is the quite stable peak around 100°E, which appears in four seasons. The wave-like longitudinal pattern of equatorial $B0$ is reported for the first time.

It has long been recognized that the tilt of the magnetic field configuration leads to the longitudinal dependence of the ionospheric parameters and their variations. However, the wave-like longitudinal dependency of $B0$ cannot be explained solely with the control of the magnetic field configuration. Recent works suggest there are possible couplings of sources with lower atmospheric origins, like the non-migrating tide mode DE3 (e.g., Kil et al., 2007; Wan et al., 2008). The modulation of the tide winds through daytime E-region dynamo effect will cause significant longitudinal variations in the equatorial vertical drift, which has been reported by Kil et al. (2007). As we know, the equatorial and low latitude ionosphere is strongly controlled by the vertical drift through the plasma fountain effect. Thus, the longitudinal structure of the vertical drift will in turn modulate that of $B0$ (the thickness of the bottomside ionosphere) in addition to N_e. The wave-like longitudinal structure has been found in daytime N_e (e.g., Lin et al., 2007; Lühr et al., 2007; Ren et al., 2008), total electron content (Wan et al., 2008), scale height (Liu et al., 2008), and even in the annual and semiannual amplitudes of equatorial N_e (Liu et al., 2009). Now we found similar wave-like structure for the longitudinal variation of $B0$ which is in agreement with the above idea.

5. Summary

We have analyzed global N_e data from the F3/C IRO observations from DoY (day number of year) 194, 2006 to DoY 293, 2008 to investigate the daytime behaviors of IRI-B parameters ($B0$ and $B1$) in equatorial regions at the low level of solar activity. In summary, the major features are outlined as follows:

(1) The IRI bottomside profile function, as given in Eq. (1), can well describe the average profiles of equatorial electron densities in the bottomside ionosphere at low solar activity.
(2) The longitudinal averaged values of $B1$ derived from observations have comparable values with IRI-2007.
(3) The observed $B0$ has semiannual variation with maxima in solstice months and minima in equinox months, which is not reproduced by IRI-2007. There is significant longitudinal variation of $B0$ with patterns varying with seasons. Wave-like structure is distinct in equinoxes with four longitudinal peaks. An interesting feature is that a stable peak appears around 100°E in four seasons. The complicated longitudinal variation of $B0$ provides challenges for further improving the presentations of the bottomside ionosphere in IRI.

Note added in proof

After this work being accepted and quequing for publication, Yue et al. (2010) made an error analysis of Abel retrieved electron density profiles from radio occultation measurements. Their result shows that the retrieved NmF2 and hmF2 are generally in good agreement with the true values, but the reliability of the retrieved electron density degrades in low latitude regions and at low altitudes. Therefore, we do not know the possible effects on the profile parameters of this possible retrieval error, which require further investigation.

Acknowledgements

This study made use of the IRO data from the COSMIC Data Analysis and Archive Center (CDAAC). This research was supported by National Natural Science Foundation of China (40725014) and National Important Basic Research Project (2006CB806306).

References

Adeniyi, J.O., Radicella, S.M. Diurnal variation of ionospheric profile parameters $B0$ and $B1$ for an equatorial station at low solar activity. J. Atmos. Solar-Terr. Phys. 60 (3), 381–385, 1998.

Altadill, D., Arrazola, D., Blanch, E., Buresova, D. Solar activity variations of ionosonde measurements and modeling results. Adv. Space Res. 42, 610–616, 2008.

Altadill, D., Torta, J.M., Blanch, E. Proposal of new models of the bottom-side $B0$ and $B1$ parameters for IRI. Adv. Space Res. 43, 1825–1834, 2009.

Batista, I.S., Abdu, M.A. Ionospheric variability at Brazilian low and equatorial latitudes: comparison between observations and IRI model. Adv. Space Res. 34, 1894–1900, 2004.

Bilitza, D. The International Reference Ionosphere 1990, National Space Science Data Center, NSSDC/WDC-A-R&S Reports 90-22, Greenbelt, Maryland, 1990.

Bilitza, D., Reinisch, B.W. International Reference Ionosphere 2007: Improvements and new parameters. Adv. Space Res. 42, 599–609, 2008.

Bilitza, D., Radicella, S.M., Reinisch, B.W., Adeniyi, J.O., Gonzalez, M.E., Zhang, S.-R., Obrou, O. New $B0$ and $B1$ models for IRI. Adv. Space Res. 25 (1), 89–95, 2000.

Blanch, E., Arrazola, D., Altadill, D., Buresova, D., Mosert, M. Improvement of IRI $B0$, $B1$ and D1 at midlatitudes using MARP. Adv. Space Res. 39, 701–710, 2007.

Chen, H., Liu, L., Wan, W., Ning, B., Lei, J. A comparative study of the bottomside profile parameters over Wuhan with IRI-2001 for 1999–2004. Earth Planet Space 58 (5), 601–605, 2006.

Gulyaeva, T.L. Progress in ionospheric informatics based on electron-density profile analysis of ionograms. Adv. Space Res. 7 (6), 39–48, 1987.

Kil, H., Oh, S.-J., Kelley, M.C., Paxton, L.J., England, S.L., Talaat, E., Min, K.-W., Su, S.-Y. Longitudinal structure of the vertical ExB drift and ion density seen from ROCSAT-1. Geophys. Res. Lett. 34, L14110, doi:10.1029/2007GL030018, 2007.

Lee, C.C., Reinisch, B.W., Su, S.-Y., Chen, W.S. Quiet-time variations of F2-layer parameters at Jicamarca and comparison with IRI-2001 during solar minimum. J. Atmos. Solar-Terr. Phys. 70 (1), 184–192, 2008.

Lei, J., Syndergaard, S., Burns, A.G., et al. Comparison of COSMIC ionospheric measurements with ground-based observations and model predictions: preliminary results. J. Geophys. Res. 112, A07308, doi:10.1029/2006JA012240, 2007.

Lin, C.H., Hsiao, C.C., Liu, J.Y., Liu, C.H. Longitudinal structure of the equatorial ionosphere: time evolution of the four-peaked EIA structure. J. Geophys. Res. 112, A12305, doi:10.1029/2007JA012455, 2007.

Liu, L., Le, H., Wan, W., Sulzer, M.P., Lei, J., Zhang, M.-L. An analysis of the scale heights in the lower topside ionosphere based on the Arecibo incoherent scatter radar measurements. J. Geophys. Res. 112, A06307, doi:10.1029/2007JA012250, 2007.

Liu, L., He, M., Wan, W., Zhang, M.-L. Topside ionospheric scale heights retrieved from Constellation Observing System for Meteorology, Ionosphere, and Climate radio occultation measurements. J. Geophys. Res. 113, A10304, doi:10.1029/2008JA013490, 2008.

Liu, L., Zhao, B., Wan, W., Ning, B., Zhang, M.-L., He, M. Seasonal variations of the ionospheric electron densities retrieved from Constellation Observing System for Meteorology, Ionosphere, and Climate mission radio occultation measurements. J. Geophys. Res. 114, A02032, doi:10.1029/2008JA013819, 2009.

Lühr, H., Häusler, K., Stolle, C. Longitudinal variation of F region electron density and thermospheric zonal wind caused by atmospheric tides. Geophys. Res. Lett. 34, L16102, doi:10.1029/2007GL030639, 2007.

Mahajan, K.K., Sethi, N.K. Empirical models of parameters *B*0, *B*1 from Arecibo radar measurements. Adv. Space Res. 27 (1), 17–20, 2001.

McKinnell, L.-A., Chimidza, O., Cilliers, P. The variability and predictability of the IRI *B*0, *B*1 parameters over Grahamstown, South Africa. Adv. Space Res. 44, 747–755, 2009.

Mosert, de G. Behavior of the IRI-B parameters for San Juan (Argentina) at midnight. Adv. Space Res. 22 (6), 753–755, 1998.

Obrou, O., Adeniyi, J.O., Kobea, A.T., Moukassa, B. Electron density profile parameters *B*0 and *B*1 response during a magnetic disturbance at equatorial latitude. J. Atmos. Solar-Terr. Phys. 67, 515–519, 2005.

Radicella, S.M., Bilitza, D., Reinisch, B.W., Adeniyi, J.O., Gonzalez, M.E., Zolesi, B., Zhang, M.-L. IRI task force activity at ICTP: proposed improvements for the IRI region below the F peak. Adv. Space Res. 22 (6), 731–739, 1998.

Reinisch, B.W., Huang, X. Finding better *B*0 and *B*1 parameters for the IRI F2 profile function. Adv. Space Res. 22 (6), 741–747, 1998.

Ren, Z., Wan, W., Liu, L., Zhao, B., Wei, Y., Yue, X., Heelis, R.A. Longitudinal variations of electron temperature and total ion density in the sunset equatorial topside ionosphere. Geophys. Res. Lett. 35, L05108, doi:10.1029/2007GL032998, 2008.

Sethi, N.K., Dabas, R.S., Singh, L., Vohra, V.K., Veenadhari, B., Garg, S.C. Results of foF2 and Ne-h profiles at low latitude using recent digital ionosonde observations and their comparison with IRI-2000. J. Atmos. Solar-Terr. Phys. 65, 749–755, 2003.

Sethi, N.K., Dabas, R.S., Upadhayaya, A.K. Midday bottomside electron density profiles during moderate solar activity and comparison with IRI-2001. Adv. Space Res. 43, 973–983, 2009.

Wan, W., Liu, L., Pi, X., Zhang, M., Ning, B., Xiong, J., Ding, F. Wavenumber-4 patterns of the total electron content over the low latitude ionosphere. Geophys. Res. Lett. 35, L12104, doi:10.1029/2008GL033755, 2008.

Yue, X., Schreiner, W.S., Lei, J., Sokolovskiy, S.V., Rocken, C., Hunt, D.C., Kuo, Y.-H. Error analysis of Abel retrieved electron density profiles from radio occultation measurements. Ann. Geophys. 28, 217–222, 2010.

Zhang, S.-R., Huang, X.-Y. Variations of bottomside electron density profile parameters obtained from observations at Wuchang, China. Adv. Space Res. 22 (6), 749–752, 1998.

Zhang, S.-R., Fukao, S., Huang, X.-Y., Otsuka, Y. The IRI's B parameters measured by the MU radar. Adv. Space Res. 25 (1), 101–104, 2000.

Zhang, S.-R., Holt, J.M., Bilitza, D., van Eyken, T., McCready, M., Amory-Mazaudier, C., Fukao, S., Sulzer, M. Multiple-site comparisons between models of incoherent scatter radar and IRI. Adv. Space Res. 39, 910–917, 2007.

Zhang, M.-L., Wan, W., Liu, L., Shi, J.K. Variability of the behavior of the bottomside (*B*0, *B*1) parameters obtained from the ground-based ionograms at China's low latitude station. Adv. Space Res. 42, 695–702, 2008.